SAND2021-1356B

Chapter 7
Molecular Design Considerations for Different Classes of Organic Scintillators

Patrick L. Feng

Abstract The purpose of this chapter is to review the distinguishing characteristics of different classes of organic scintillators with respect to the performance requirements of typical use cases. Discussion of the relevant physical and photophysical parameters will be provided in the context of the rational design of radiation detection materials. A partial list of these properties is as follows: scintillation light yield, emission wavelength and anisotropy, timing characteristics, ionizing particle discrimination, optical attenuation length, mechanical and environmental robustness, detector volume, and cost. Material design considerations relative to these properties is one of the main objectives of this Chapter.

Aromatic materials can produce scintillation light in response to ionizing radiation. This characteristic has been observed in crystalline, liquid, and amorphous scintillators, owing to a process that includes ionization recombination, population of excited electronic states, and radiative de-excitation. Organic scintillators from each category are employed today to satisfy the specific requirements of a wide range of applications.

The photophysical and scintillation properties of molecules used in organic scintillators vary across a wide range. This has resulted in over 70 years of research aimed at developing scintillators that possess specific physical and scintillation characteristics. In 1956, Sangster and Irvine Jr. published an in-depth survey describing the scintillation properties of more than fifty organic molecular crystals [1]. This work was significant since it described several important considerations that continue to govern contemporary scintillator development efforts: (1) the scintillation efficiency is dependent upon the electronic structure and fluorescence properties of the constituent molecules, (2) the orientation, shape, and steric properties of the molecule impact the mechanisms of energy transfer giving rise to scintillation, (3) the scintillation efficiency is sensitive to defects and the presence of molecular impurities. Later studies also addressed practical considerations such as detector

P.L. Feng
Sandia National Laboratories, Livermore, CA, USA
plfeng@sandia.gov

DOI

fabrication/scale-up and the relationship between molecular structure and mechanical properties. These categories provide a general framework from which to approach the development of improved organic scintillators.

7.1 Design Considerations for Crystalline, Plastic, and Liquid Scintillators

7.1.1 Background on Scintillation Mechanisms

The first organic scintillator was discovered in 1947, when Kallman reported that single crystals of naphthalene[1] produced light in response to gamma rays [2, 3]. Anthracene and *trans*-stilbene crystals were later evaluated and found to exhibit similar behavior, yet with a much higher light output response [4, 5]. These observations established the generality of scintillation response in fluorescent organic compounds. In consideration to this finding, the uniform composition and structural order of organic single crystals provided an excellent platform from which to study basic scintillation phenomena. This allowed for systematic studies on the effects of chemical and structural variation. One example is the planar series benzene-naphthalene-anthracene. Another example constitutes the *para*-polyphenyl series: biphenyl, *p*-terphenyl, and *p*-quaterphenyl. In these examples, the scintillation efficiency was found to relate to extent of charge-separation and the corresponding electron transition probabilities, with the more conjugated and larger molecules being more efficient scintillators [1]. Following the initial reports of scintillation in molecular organic crystals, it was later discovered that crystals of *trans*-stilbene could also be used to discriminate between different particle types based on the kinetics of the scintillation pulse, i.e. the method of Pulse-Shape Discrimination (PSD). While methods for the measurement of PSD is discussed in detail elsewhere (see Chap. 2, 5 and 10), the photophysical processes involved in this capability will be described herein [6-8].

All organic scintillators undergo the same primary processes of excitation and ionization that precedes scintillation light generation. According to seminal work by Birks and others, this includes four processes: (1) excitation into excited π-electron singlet states, (2) ionization of π-electrons, (3) direct excitation of σ-electron and carbon 1s electron excited states, and (4) ionization of electrons other than π-electrons [9]. Processes (1) and (2) account for the scintillation yield, with the majority of light being produced through process (1). Nonradiative pathways (3) and

[1] Topological representation and key information of these molecules is given in the Appendix section at the end of the book.

(4) do not contribute to scintillation emission but are instead associated with relaxation via thermalization and molecular damage, respectively. Thus, only the radiative processes (1) and (2) will be discussed here.

Although processes (1) and (2) involve complex theoretical underpinnings that depend on the specific organic medium, it is important to note that nearly the entirety of all organic scintillator developments can be summarized into the optimization of these two light production pathways.

7.1.2 Process (1): Direct Excitation into π-Electronic States

7.1.2.1 Process (1): Direct Excitation in Molecular Crystals

In primary (single-component) scintillators such as molecular crystals, process (1) occurs with an efficiency that is roughly proportional to the fraction of aromatic (π) electrons in the molecule and the fluorescence quantum yield (Φ_f). This explains why the scintillation light yield of the polyphenyl series benzene, naphthalene, anthracene, progressively increases in accordance with the respective quantum yields [1]. The Stokes shift is another parameter that must be considered in molecular crystals, due largely to the single-component nature of these scintillators. The Stokes shift is defined as the difference between maximum positions of the absorption and emission spectra corresponding to the same electronic transition (a formula is given in Chap. 1). A more precise description of this consideration from the perspective of scintillator design is the extent of spectral overlap between the electronic absorption and emission spectra. A nonzero spectral overlap will lead to radiative self-absorption, which has several detrimental effects: (1) size-dependent scintillation light yield, (2) shifts in the emission spectrum as a function of interaction position, also known as the 'inner filter' effect, (3) slowing down/smearing of the scintillation timing characteristics. One exception to these observations is to introduce an acceptor molecule to reduce or eliminate the spectral overlap. This can be accomplished in crystals by co-crystallizing structurally similar yet photophysically distinct dopant molecules. An example is a mixed crystal of *trans*-stilbene and 1,2-diphenylacetylene, which leads to a larger effective Stokes shift due to energy transfer from the 1,2-diphenylacetylene donor to the *trans*-stilbene acceptor molecules [10]. However, wavelength-shifted molecular crystals are rare due to the lack of suitable dopants that possess the required structural and electronic properties to be co-crystallized at uniform concentration in the sizes required for practical scintillators. The next two sections describe the practical application of this concept to multi-component solid and liquid scintillator matrices, respectively.

7.1.2.2 Process (1): Direct Excitation in Multi-component Solid-state Scintillators

In high-viscosity multi-component scintillators such as plastics and organic molecular glasses, process (1) also occurs but with additional energy transfer steps between the π-electron singlet excited states. These processes are dominated by non-radiative (i.e. Förster Resonance Energy Transfer, FRET, see also Chap. 5) but also includes radiative energy transfer via light absorption and re-emission. FRET involves the transfer of excited-state electronic energy from a donor molecule to an acceptor molecule according to a dipole-dipole coupling mechanism [11]. This process is well-known and proceeds according to the Förster equation:

$$E = \frac{1}{1 + (r/R_0)^6} \tag{7.1}$$

with R_0 being the distance between a donor and acceptor molecule at which the energy transfer efficiency is 50 %, also known as the Förster distance. Large Förster distances are associated with donor-acceptor pairs that exhibit efficient energy transfer. The Förster distance depends on several factors according to the following equation:

$$R_0^6 = \frac{2.07}{128\pi^5 N_A} \frac{\kappa^2 Q_D}{\eta^4} \int f_D(\lambda)\varepsilon_A(\lambda)\,\lambda^4 d\lambda \tag{7.2}$$

where Q_D is the fluorescence quantum yield of the donor in the absence of the acceptor, κ^2 is the dipole orientation factor, η is the refractive index of the medium, N_A is the Avogadro constant, and J is the spectral overlap integral. κ is given by:

$$\kappa = \hat{\mu}_A \cdot \hat{\mu}_B - 3\left(\hat{\mu}_D \cdot \hat{R}\right)\left(\hat{\mu}_A \cdot \hat{R}\right) \tag{7.3}$$

where $\hat{\mu}_D$ is the normalized transition dipole moment of each fluorophore, and $\hat{R}$ denotes the normalized inter-fluorophore displacement. Typically, κ^2 is assumed to be ⅔ for systems where the donor and acceptor molecules are freely rotating and considered to be isotropically oriented during the excited-state lifetime. This is true in matrices that comprise liquids, amorphous plastics, and molecular organic glasses. Returning to Eq. (7.2) above, the integral $\int F_D(\lambda)\varepsilon_A(\lambda)\,\lambda^4 d\lambda$ is associated with the spectral overlap integral, J according to:

$$J = \frac{\int f_D(\lambda)\varepsilon_A(\lambda)\lambda^4 d\lambda}{\int f_D(\lambda)\,d\lambda} = \int \overline{f_D}\,(\lambda)\varepsilon_A(\lambda)\lambda^4 d\lambda \tag{7.4}$$

where f_D is the donor emission spectrum, $\overline{f_D}$ is the donor emission spectrum normalized to an area of 1, and ε_A is the acceptor molar extinction coefficient.

The FRET efficiency not only governs the steady-state emission characteristics, but also directly controls the emission timing properties according to Eq. (7.5):

$$k_{ET} = \left(\frac{R_0}{r}\right)^6 \frac{1}{\tau_D} \tag{7.5}$$

where k_{ET} is the rate of energy transfer from the donor to acceptor and τ_D is the fluorescence lifetime of the donor. The donor-acceptor energy transfer rate (k_{ET}) controls the fluorescence/scintillation rise-time (τ_{rise}), whereas the acceptor decay time (τ_A) controls the fluorescence/scintillation decay time (τ_{em}).

With reference to the processes and equations discussed above, it is possible to come up with a set of generalized design rules guide the development of high light yield multi-component organic scintillators (Table 7.1). To this end, Berlman tabulated the photophysical characteristics of a large number of donor and acceptor molecules, including the Förster Distance (R_0), fluorescence lifetime, and quantum yield [12, 13]. Adadurov et al. performed simulations using these parameters in the above equations to optimize the composition of a plastic scintillator based on polystyrene and 1,5-bis(2-(5-phenyloxazolyl)-benzene (POPOP) [14]. The results showed the effect of wavelength shifter concentration on the light yield and optical attenuation length, as shown in Fig. 7.1.

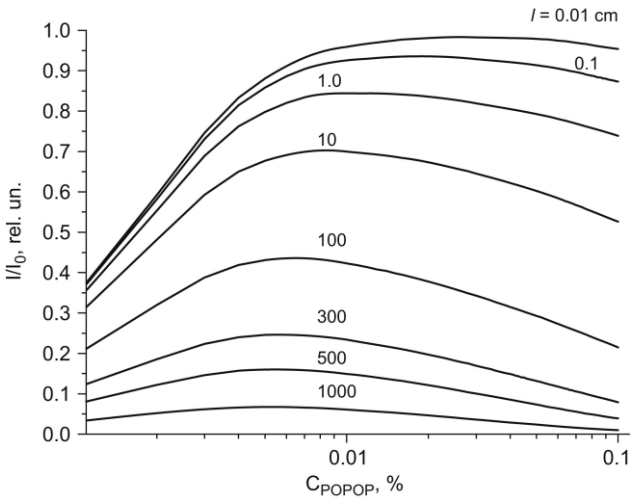

Fig. 7.1 Relative intensity of luminescence for different POPOP concentrations and optical path lengths (l) in polystyrene plastic scintillator (reproduced from [14] with permission from Elsevier)

Table 7.1 Summary of relevant photophysical parameters contributing to the design of high light-yield multi-component organic scintillators

Parameter Symbol	Parameter Description	Design Criteria	Rationale	Strategy
E	FRET Energy Transfer Efficiency	Maximize	Improve scintillation light yield	(See parameter entries below)
R_0	Förster Distance	Maximize	Increase E	(See parameter entries below)
Q_D	Donor Quantum Yield	Maximize	Increase R_0 and E	Select highly fluorescent host matrix
ε_A	Acceptor oscillator strength	Maximize	Increase Spectral Overlap	Ensure large acceptor oscillator strength
$\int Q_D(\lambda)\varepsilon_A(\lambda)\lambda^4 d\lambda$	Spectral Overlap	Maximize	Increase R_0 and E	Match donor emission and acceptor absorption spectra
κ^2	Orientation Factor	Maximize	Increase R_0 and E	Impose isotropic molecular orientations
$\int f_A(\lambda)\varepsilon_A(\lambda)\lambda^4 d\lambda$	Self-Absorption	Minimize	Long optical attenuation length	Maximize acceptor Stokes' shift
τ_D	Donor scintillation decay time	Minimize	Increase R_0, fast rise-time	Select donor that has short emission lifetime
τ_A	Acceptor scintillation decay time	Minimize	Fast decay time	Select acceptor that has short emission lifetime
Q_A	Acceptor Quantum Yield	Maximize	Increase scintillation light yield	Select highly fluorescent acceptor(s) (i.e. primary and secondary fluorophores)

One notable characteristic of plastic scintillators is that their light yields are lower than the brightest molecular crystals and liquid scintillators by ~ 50 % and ~ 20 %, respectively [15, 16]. This is due in large part to the finite donor quantum yields and maximum achievable FRET efficiency of existing polymer hosts reported to date. Liquid scintillators also possess this limitation but are generally more efficient than plastics due to an enhancement in the energy transfer efficiency via molecular diffusion.

7.1.2.3 Process (1): Direct excitation in Liquid Scintillators

In low-viscosity multi-component materials such as liquid scintillators, the mechanisms of energy transfer in liquids is similar to that of high-viscosity media such as plastics and glasses but is also influenced by translational diffusion (D). The solvent viscosity controls the diffusion rate to establish a displacement distance (R_D) that occurs on the FRET timescale. The donor-acceptor energy transfer efficiency in

liquid solutions thus depends on the relationship between the Förster radius (R_0) and the displacement distance (R_D). In other words, shorter R_0 distances may be overcome by fast diffusion via low viscosity/large R_D, and vice versa. This relationship has been demonstrated in prior work, whereby the solvent viscosity was shown to modulate the efficiency of fluorescence energy transfer [17]. This effect was revealed by studying different donor-acceptor pairs that were subject to cooling or solvent substitution. A summary of the parameters and design considerations controlling the efficiency of donor-acceptor energy transfer in liquids is provided in Table 7.2.

7.1.2.4 Summary of Process (1) Effects

The impact of process (1) to the above material categories may be summarized by the following generalizations:

- Organic single crystals exhibit the highest scintillation light yields due to high fluorescence quantum yields.
- Multi-component scintillators provide superior optical attenuation lengths due to reduced absorption/emission spectral overlap, as enabled by FRET.

No crystalline, liquid, or plastic scintillator provides an ideal solution towards high light-yield and long attenuation length scintillators, due to the requirements for direct π-excitation (process (1)). Consequently, a key objective constitutes a multi-component scintillator that has high donor fluorescence quantum yield and efficient donor-acceptor FRET.

We may now turn our attention to process (2) to complete the description of light-generation pathways in organic scintillators.

Table 7.2 Summary of photophysical parameters contributing to the design of high light-yield liquid scintillators. Liquid scintillators are generally categorized as multi-component and low viscosity materials

Parameter Symbol	Parameter Description	Design Criteria	Rationale	Strategy
η	Solvent Viscosity	Minimize	Increase diffusion rate (D) and displacement (R_D)	Select low-viscosity liquid scintillator matrix
D	Diffusion constant	Maximize	Increase R_D	Select low-viscosity liquid scintillator matrix
R_D	Displacement distance	Maximize	Relaxes requirement of large R_0 value	Select low-viscosity liquid scintillator matrix
FRET	Förster Resonance Energy Transfer	Maximize	Increase efficiency of radiation emission on diffusion timescale	Increase Förster Distance (R_0) (See Table 7.1)

7.1.3 Process (2): Overview of Direct Ionization and Recombination of π-states

While the majority of scintillation light output (e.g. ~ 80 %) occurs due to excitation into excited π-electron singlet states via process (1), ionization of π-electrons via process (2) contributes to an important part of the light pulse that is essential for applications that require particle discrimination. Following ionization of π-electrons, ion recombination leads to the population of both singlet and triplet excited states with a ¼ and ¾ ratio, respectively. The excited singlets produced by process (2) decay in accordance with the fluorescence decay time and add to the prompt scintillation response produced by process (1). The triplet excited states formally cannot decay to the ground state due to spin-parity selection rules and may either thermalize or annihilate with another excited triplet if the excitation density is sufficiently high. The latter process is called Triplet-Triplet Annihilation (TTA). TTA accounts for the delayed part of the scintillation response and enables pulse-shape discrimination (PSD) techniques to be used.

The efficiency of TTA depends on the mobility and lifetime of the triplet excited states, which correlates closely with the molecular structure and electronic properties of the scintillator. TTA occurs via Dexter energy transfer via triplet wavefunction overlap and is described by Eq. (7.6).

$$k_{ET} \propto Jexp\left[\frac{-2r}{L}\right] \tag{7.6}$$

In this equation, k_{ET} is the Dexter energy transfer rate, J is the spectral overlap integral for triplet states, r is the separation between donor and acceptor, and L is the sum of the Van der Waals radii of the donor and acceptor. k_{ET} determines the efficiency at which TTA can occur, which in turn controls the quantity and kinetics of the delayed scintillation response. Due to the exponential distance dependence in Eq. (7.6), Dexter energy transfer/TTA is a short-range process that is operative at distances of less than 1 nm. This contrasts with the dipolar FRET mechanism that occurs at longer distances of 1-10 nm. Consequently, TTA is more sensitively impacted by the presence of impurities, disorder, or other defects. The relative impact of these considerations will be discussed in the following sections for different classes of organic scintillators.

7.1.3.1 Process (2): Direct Ionization and Recombination in Molecular Crystals

There are several considerations that impact the probability for Dexter energy transfer via TTA in organic molecular crystals. The most fundamental considerations are the electronic structure of the organic compound constituting the crystal. A wide

variation in PSD capability was reported in work by Galunov et al. and Hull et al. for a diversity of organic crystals.[add references from comment at right] However, there are additional factors that impact the TTA efficiency in crystals of a particular compound. These considerations principally include the compositional purity, degree of crystallographic order, and symmetry effects. These properties also affect the electronic properties of the system, namely the presence of triplet trap levels that reside between the HOMO and LUMO of the pure host material.

Purity

Efforts to improve the PSD capabilities of organic crystals have generally focused on decreasing the triplet exciton trap density via extensive purification and higher structural perfection. Arulchakkaravarthi studied the scintillation properties of melt-grown *trans*-stilbene crystals of varying degrees of structural order, as assessed by X-ray rocking curve analysis [18]. This study found that an increased concentration of low angle grain boundary defects decreased the amount of delayed fluorescence and consequently led to poorer PSD. In subsequent work, solution-grown *trans*-stilbene crystals were found to possess better pulse-shape discrimination properties than melt-grown *trans*-stilbene, owing to a higher degree of structural perfection and more efficient TTA [19]. Solution crystal growth methods impose fundamental limitations on the growth rate and mechanical toughness of the crystal (see section 7.1.4.1), which in turn influences the maximum practical crystal size, production yield, and cost.

Mixed Crystals

An exception to the ‘purer is better’ approach outlined above comprises co-crystallization of two structurally similar molecules that possess different electronic properties. For example, Zaitseva et al. investigated the scintillation properties of mixed single crystals [10]. 1,2-Diphenylacetylene (‘DPAC’) was co-crystallized with *trans*-stilbene (‘stilbene’) at concentrations of 2-55 %. It was discovered that TTA was nearly completely suppressed for a 98:2 crystal of DPAC:stilbene, as might be expected due to the presence of a sufficient trap density to quench the triplet excitons required for TTA. However, TTA was restored in a 63:37 DPAC:stilbene co-crystal such that the PSD capabilities of the mixed crystal exceeded either of the pure constituent crystals. This surprising result was attributed to a sufficient concentration of deep traps in the crystal to facilitate efficient trap-to-trap hopping above the triplet percolation threshold. This result is consistent with earlier work by Robinson, who reported that TTA is maximized in systems that contain a low concentration of shallow traps or a high concentration of deep traps [20]. The distinction between shallow and deep in this context refers to the trap depth with respect to the LUMO and the relative thermal energy of the radiationless transition (kT).

Crystallographic Symmetry

Another strategy that has been employed to increase the efficiency of TTA involves the molecular design of scintillators that crystallize in high-symmetry space groups. As stated previously, TTA is dependent upon the concentration, lifetime, and mobility of triplet excitons. The triplet concentration is established by the ionization event itself, whereas the triplet lifetime is controlled by the electronic properties of the triplet state and purity of the crystal. The remaining factor, triplet mobility, is a second rank tensor property that is intrinsically symmetry dependent [21]. Higher-symmetry systems exhibit greater triplet mobility relative to their low-symmetry analogs, as previously reported for a series of naphthalene- and salicylate-based organic crystals [22]. In that work, efficient TTA and excellent PSD were observed in crystals of higher symmetry analogs of monoclinic compounds that do not themselves exhibit PSD. Density-functional theory calculations revealed that the intermolecular triplet-excitation energy transfer interactions in a trigonal naphthalene crystal were more than twelve times larger than its lower-symmetry monoclinic analog.

Other studies confirm the role of symmetry on the magnitude and angular dependence of the transport mobility. Vehoff et al. studied the charge-transporting properties of crystallographic polymorphs of benzo[1,2-*b*:4,5-*b′*]bis[*b*]benzothiophene, whereby an order-of-magnitude larger charge transport mobility was observed for the 3-dimensional versus 1-dimensional molecular network [23]. Separately, the effect of crystallographic symmetry upon the scintillation light yield and PSD anisotropy was evaluated [24, 25]. Angular-dependent neutron measurements on monoclinic *trans*-stilbene crystals revealed uncorrelated angular dependencies for the light output and PSD performance. The extent of variation was ~ 20 % in light output and ~ 10 % in PSD from respective minimum to maximum (Fig. 7.2) [24, 25].

Another property related to symmetry and triplet transport is the percolation threshold. This threshold is a mathematical property that describes the concentration of a dopant or impurity at which an infinite cluster appears for the first time in an infinite lattice. A visual example of the percolation threshold is provided for a 2D square lattice in Fig. 7.3. In this figure, the percolation threshold corresponds to the site occupancy at which connectivity throughout the system is achieved. This concentration is $X \geq 0.6$ for a 2D square lattice. Table 7.3 provides the percolation thresholds for different crystal lattice types, where X refer to the dopant concentrations at which percolation transport is enabled [26]. From these data, it is clear that percolation thresholds are lowered in high-symmetry structures, which relaxes the minimum crystal purity and structural order requirements that are needed for TTA. The highest symmetry face-centered cubic (fcc) lattice type corresponds to the lowest percolation threshold concentration due to the largest number of spatially degenerate states. Unfortunately, 80 % of known organic crystals are triclinic or monoclinic, with less than 0.1 % of known organic crystals belonging to cubic space groups.

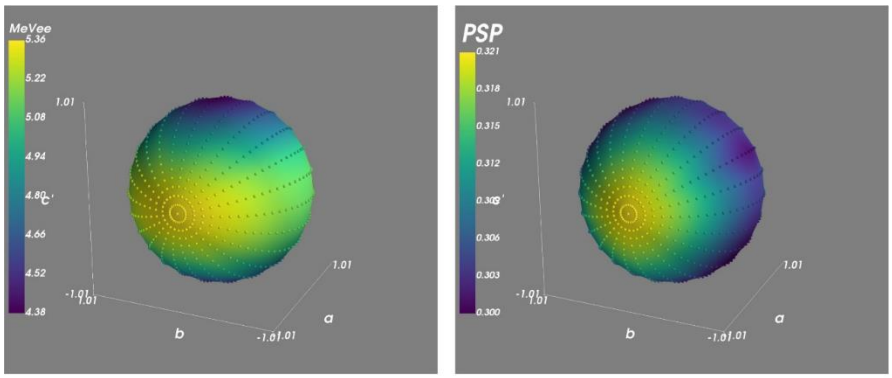

Fig. 7.2 Anisotropy of **a** the light output and **b** pulse shape parameter for 10 MeV recoil protons plotted relative to the crystal axes of *trans*-stilbene (reproduced from [24] with permission from Elsevier)

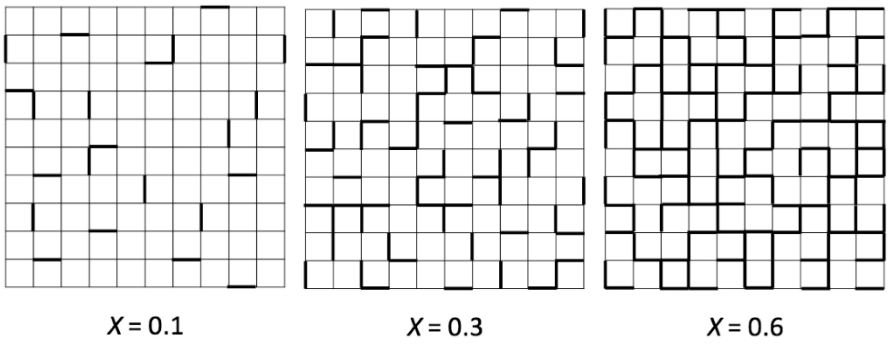

Fig. 7.3 Percolation in a 2D square lattice with occupation probabilities of X = 0.1, 0.3, and 0.6, respectively. Percolation occurs through the lattice at X ≥ 0.6 (reproduced from [27] with permission from Elsevier)

Considering this limitation, crystal engineering was evaluated as a strategy to high-symmetry organic scintillator crystals [22]. In 2013, Feng and Foster designed three-fold symmetric organic molecules intended to serve as a structure-directing element for the C_3 symmetry element that is present in trigonal, hexagonal, and cubic crystal systems. Fluorescent naphthalene and salicylic acid chromophore groups were attached to a non-luminescent trialkoxyamine core structure, leading to high-symmetry versions of monoclinic naphthalene and salicylic acid crystals. The result was a 'turning on' of PSD capabilities through enhanced triplet excitation energy transfer, as shown in Fig. 7.4. Density-Functional Theory calculations veri-

Table 7.3 Percolation threshold values for different crystal lattice types [26]

Dimension	Lattice Type	Site Threshold Value (X)
2	Triangle	0.500
2	Square	0.593
2	Honeycomb	0.698
3	Face-centered cubic	0.198
3	Body-centered cubic	0.245
3	Simple cubic	0.311
3	Diamond	0.428

fied a twelve-fold increase in triplet-triplet exchange interactions for tris(1-naphthyloxy)triethylamine, when compared to its low-symmetry parent compound naphthalene.

The three methodologies outlined above (purity, mixed crystals, crystallographic symmetry) represent proven strategies towards improved PSD in crystalline organic scintillators. However, all of these approaches are associated with scientific and practical challenges that generally constrain the use of organic crystals to small-scale applications with scintillator volumes of a few cubic inches or less.

7.1.3.2 Process (2): Direct Ionization and Recombination in Plastic Scintillators

The first plastic scintillators were reported in 1950 by Schorr and Torney and have progressed over the intervening decades to meet the need for low-cost, large-scale, and/or mechanically robust organic scintillators [28 and Chap. 1]. However, even after more than seventy years of development, the scintillation light yield and PSD properties of commercial plastic scintillators remain inferior to liquid and crystalline scintillators. The reasons for the lower scintillation light yield are related to limitations in process (1), i.e. the FRET energy transfer efficiency. The present section is concerned with a discussion of the reasons for inefficient process (2) energy conversion that is the root cause of the limited PSD properties of plastics.

Plastic scintillators are based upon an aromatic-containing polymer base in which fluorescent solutes are dissolved (or sometimes covalently linked to the polymer chain). Polystyrene (PS) and poly(vinyltoluene) (PVT) are the most commonly used polymers, due to their high aromatic content, low cost, and favorable thermomechanical properties. These host matrices are linear polymers that are characterized as glassy thermoplastics. Thermoplastic behavior refers to a change in physical properties (e.g. hardness and flow characteristics) above its glass transition temperature without an associated phase change. This behavior is associated with

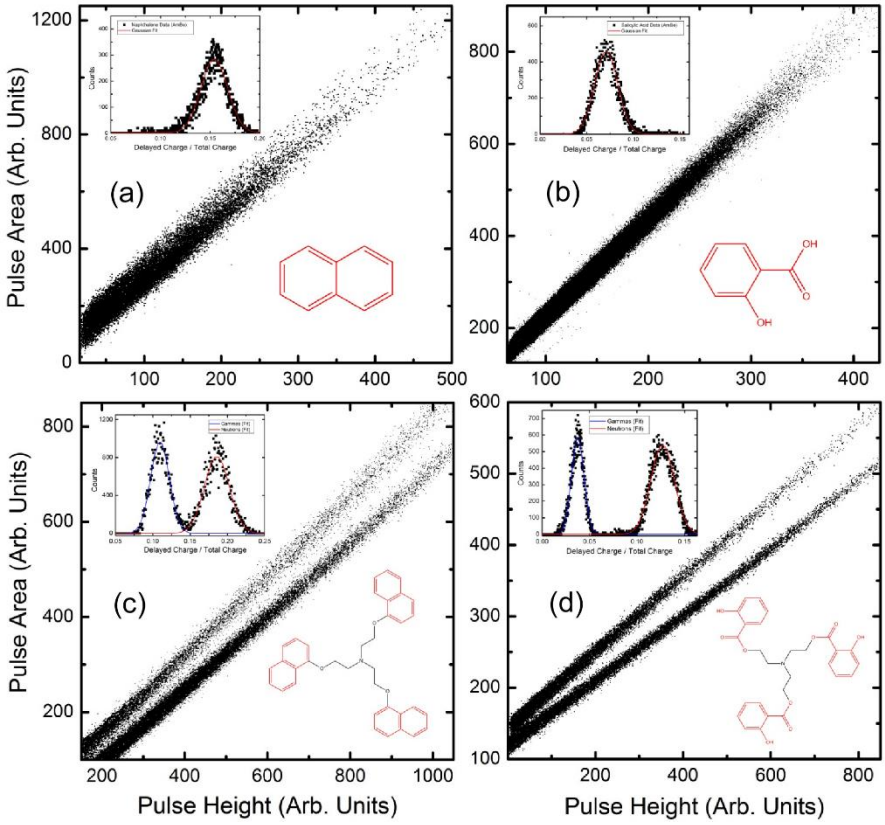

Fig. 7.4 Comparison of the neutron/gamma PSD properties of low-symmetry crystals naphthalene (top left) and salicylic acid (top right) with their high-symmetry trialkoxyamine analogs (bottom left and bottom right), respectively (reproduced from [22] with permission from IEEE)

the high molecular weight of PS and PVT used in scintillators, which leads to entanglement of the long polymer chains. Chain entanglement is favorable for promoting good mechanical strength and isotropic optical properties, but it also results in polydispersity with respect to chain length and molecular orientations.

Polydispersity leads to a broad distribution of molecular environments that introduces significant disorder and exciton trapping sites. Chen et al. performed density-functional theory calculations of polystyrene to assess the effect of disorder upon the electronic properties of polystyrene [29]. Those findings revealed that morphological disorder leads to the formation of shallow and deep traps near the band edges of the polymer. This accounts for a significant triplet exciton deactivation pathway due to the intrinsically disordered nature of polystyrene. Another potential triplet trapping pathway comprises excimer formation in PS and/or PVT. Excimers are excited state dimers that form between identical aromatic molecules due to π-π orbital overlap. Polystyrene is known to exhibit monomer as well as excimer

emission depending on the polymerization method and thermal history [30-32]. Excimer formation and TTA have been shown to be competitive in aromatic materials since both pathways serve to depopulate triplet excited states [33-36]. As a result, conventional plastic scintillators based on linear PS and PVT exhibit minimal delayed fluorescence due to TTA and are not capable of any significant PSD.

PSD Plastics

In 1960, Brooks overcame the constraints of triplet trapping in plastic scintillators by incorporating higher concentrations than usual of naphthalene or 4-isopropylbiphenyl in PVT [37]. This behavior has been explained by a similar mechanism as described for mixed organic crystals, namely the introduction of dye molecules to facilitate TTA via trap-to-trap hopping transport [10]. In light of this ground-breaking result, it is surprising that no subsequent work was published on PSD plastics for a period of more than fifty years. This may be due to the limited stability of dissolved small molecules such as naphthalene and 4-isopropylbiphenyl in PVT. In 2012, Zaitseva et al. reported efficient PSD in PVT plastic scintillators that were loaded with 2,5-diphenyloxazole (PPO) at concentrations of up to 30 wt% [38]. The best PSD performance was comparable to EJ-301 liquid and was achieved for the highest attainable PPO loading of 30 wt%. Initial results indicated that PPO was less susceptible to recrystallization in PVT than other studied molecules such as naphthalene, although later work showed that PPO recrystallization could still occur under ambient conditions [37, 39]. Recrystallization occurred due to the high molecular mobility of PPO in the plasticized PVT matrix, as reflected by the low glass transition temperatures and soft/rubber-like physical characteristics at room temperature [40]. Cross-linking or the co-polymerization of monomeric PPO compounds in PVT were found to be effective in improving the physical characteristics and suppressing PPO recrystallization, although both of these strategies have practical implications for cost, production throughput/yield, and long-term stability [41, 42].

Subsequent work investigated highly soluble small-molecule alternatives to PPO [43], including functionalized *p*-terphenyl and fluorene derivatives [44]. However, results to date show that PPO loading yields the best PSD capabilities [39]. Grodzicka-Kobylka et al. [45] and Sénoville et al. [46] both compared the PSD and light yields of commercial PSD plastic scintillators (Eljen Technology EJ-299-33(G), EJ-299-34(G), and their replacement EJ-276) against EJ-301 liquid scintillator. The results reveal light yield and neutron/gamma PSD discrimination properties that lag behind EJ-301 across the measured energy range. These limitations provide a motivation for continued scintillator development efforts.

7.1.3.3 Process (2): Direct Ionization and Recombination in Liquid Scintillators

The mechanism for TTA in liquid scintillators is different from the solid-state materials discussed above in that it involves fast molecular diffusion. Diffusion enables the minimum primary fluorophore concentration in liquids to be low, on the order of 2 wt% for typical scintillation mixtures based on aromatic liquids such as 1,2,4-trimethylbenzene (pseudocumene). This primary fluorophore concentration is roughly an order of magnitude less than in plastic scintillators. At this concentration, the triplet excited state lifetimes and molecular diffusion rate are large enough to facilitate efficient bimolecular recombination via TTA. However, the diffusion rate is inversely proportional to the viscosity and molecular size according to the Stokes-Einstein given in Eq. (7.7),

$$D = \frac{k_B T}{6\pi r \eta} \tag{7.7}$$

where D is the diffusion coefficient, k_B is the Boltzmann constant, r is the radius of a moving particle, and η is the solvent viscosity. It is clear from this relationship that TTA cannot be enhanced by fast diffusion in high-viscosity solid-state scintillator matrices as it is for liquids. Another property of liquid scintillators that reflects the role of fast diffusion towards TTA pertains to the effect of dissolved oxygen. Liquid scintillators must be rigorously deoxygenated since the paramagnetic nature of O_2 quenches triplet excited states. The rate of quenching is competitive with TTA and results in the loss of PSD capabilities for solutions exposed to oxygen from the atmosphere. Liquids thus possess strict packaging requirements to prevent oxygen ingress and/or solvent egress.

Based on the above considerations for crystals, plastics, and liquids, the ideal organic scintillator matrix is one that has a high fluorescence quantum yield in the ultraviolet range, is molecularly monodisperse, packs isotropically, and is high viscosity/solid-state. These attributes refer specifically to the photophysical and energy transfer properties. We may now turn to a discussion of the physical and mechanical properties of different organic scintillators.

7.1.4 Physical and Mechanical Properties of Different Classes of Organic Scintillators

7.1.4.1 Crystallographic Structure Effects in Molecular Crystals

A characteristic of crystalline organic scintillators is that virtually all known examples crystallize in monoclinic space groups in a herringbone or double herringbone configuration. This commonality supports systematic comparison studies but imposes restrictions on properties that are symmetry-dependent. Second-rank tensor

properties are intrinsically symmetry-dependent and include mobility, thermal conductivity, and thermal expansion coefficient, among others. Indeed, the TTA mobility was discussed in the preceding section for low-symmetry versus high-symmetry versions of organic crystals [22]. Stress and strain response are also second-rank tensors, which relates to physical properties such as hardness and fracture toughness.

Prior work has established the relationship between the solid-state packing and the mechanical properties of molecular crystals [47]. The core design requirement for optical materials such as scintillators is that the applied stress (force/unit area) must not exceed the strength of the crystals; otherwise, it leads to deformation or fracture failure. Most organic crystals, including scintillators such as anthracene and *trans*-stilbene, exhibit brittle behavior. This is characterized by failure due to fracture rather than by plastic deformation. In anthracene and *trans*-stilbene, fracture preferentially occurs along the basal crystallographic cleavage plane in response to thermal or mechanical stresses that exceed the crystal's yield strength. One mitigation to this failure mode involves enhanced fracture toughness via plastic flow. This concept was first theorized by Tresca in 1864 and later developed into a classical theory by Prager and Hill. Their work indicates that plastic flow occurs in molecular crystals via the movement of edge dislocations and grain boundaries [48-50]. Indeed, high dislocation densities in metals and organic crystals have been shown to increase the ductility and fracture toughness of the crystal [51, 52]. Conventionally-grown Bridgman *trans*-stilbene crystals have been shown to have a high density of edge dislocations and low angle grain boundaries, which toughens the crystal relative to a more defect-free specimen grown via the selective-self seeding vertical Bridgman technique (SSVBT) or solution-growth methods. Unfortunately, the presence of dislocations and low-angle grain boundary defects have been shown to negatively impact the scintillation properties due to disruption of intermolecular dipolar and electronic exchange interactions [18, 53]. This observation reveals a trade-off between the scintillation performance of *trans*-stilbene single crystals and their susceptibility to failure due to fracture. To demonstrate this point, we may consider solution-grown *trans*-stilbene. Crystals grown by this method have been shown to provide the highest scintillation performance, owing to their high degree of compositional and structural uniformity [19]. However, solution-grown *trans*-stilbene crystals are susceptible to mechanical and thermal shocks, as evidenced by a maximum manufacturer-recommended thermal gradient of no more than 10 °C/hour and 5 °C/hour for 1" × 1" and 2" × 2" cylinders, respectively [54].

7.1.4.2 Physical Properties of Plastic Scintillators

Three of the key physical limitations of organic crystals can be summarized as: anisotropic optical/mechanical properties, brittle characteristics, and difficulty in scaling to large sizes. These issues are essentially overcome in plastic scintillators due

to a disordered arrangement of covalently-bonded polymer chains. The random tangling of polymer chains used in plastic scintillators results in amorphous character with no preferred molecular orientations. This attribute leads to an isotropic refractive index, which is desirable to achieve uniform detector response and light collection from bulk scintillator elements. The combination of inter-chain entanglement and the covalent nature of polymer bonds also leads to mechanically robust materials. This is reflected in glass transition temperatures that are significantly above room temperature (e.g. ~ 95 °C for PVT) and mechanical properties that are suitable for large-scale or structural applications [55]. Furthermore, commercial plastic scintillators are produced using thermally-induced radical polymerization of liquid monomer, which is amenable to large-scale production and the incorporation of functional additives such as primary fluorophores and wavelength shifters (see Chap. 1 for more information on the preparation of plastic scintillators).

However, the use of polymers introduces a different set of limitations not observed in crystalline or liquid materials. For example, chain entanglement introduces microscopic void volumes due to packing inefficiencies. This has consequences for applications that are subject to atmospheric moisture and/or gaseous radioactive isotopes. In outdoor deployments such as in radiation portal monitors, water vapor diffuses into plastic scintillators, which leads to temporary and permanent 'fogging' following changes in the ambient temperature [56-59]. Similarly, radioactive noble gases produced by nuclear explosions and subject to monitoring within the Comprehensive Nuclear-Test-Ban Treaty (CTBT), may diffuse into plastic scintillators. This leads to an undesired 'memory effect' that comprises a rising background level over time [60, 61].

Triplet trapping and the loss of PSD capabilities is another issue with plastic scintillators, as discussed above. This constraint may be mitigated by adding high concentrations of a primary dye, although this plasticizes the matrix and results in soft/'rubber-like' properties. For example, incorporating PPO at concentrations of 15-30 wt% in PVT leads to mechanically deformable materials that possess glass transition temperatures that are near or below room temperature [40, 62]. Lim et al. reported an 88 % reduction in the 25 °C Shore D hardness for PVT-based scintillators loaded with ≥ 20 wt% of PPO [40]. Cross-linking to produce a thermo-set polymer has been effective in increasing the mechanical hardness at high dye concentrations, although cross-linked samples retain low glass transition temperature (T_g) values and high attendant molecular mobility/diffusion of dissolved dye molecules [62, 63]. Diffusion of the dissolved scintillator constituents over time may lead to degradation of the scintillation light yield and PSD properties over time [64].

7.2 Future Opportunities

The preceding sections describe the advantages and limitations of different classes of organic scintillators. Existing organic scintillators are characterized by a complex

set of trade-offs that must be weighed against the requirements for each intended application. These factors include practicality versus performance considerations associated with each scintillator type. Consideration of the extensive literature to date reveals several landmark advances towards bright, fast, and PSD-capable crystalline, liquid, and plastic scintillators, while providing multiple pathways towards further improvements. For example, scintillation light yields for the brightest plastic and liquid scintillators lag behind crystalline materials such as *trans*-stilbene and anthracene due in large part to the low fluorescence quantum yield of the host material. Consequently, an ongoing objective is to develop high quantum yield host materials as replacements for PVT polymer and existing aromatic solvents, respectively. Furthermore, analysis of the Förster equation reveals further opportunities to increase the host-guest energy transfer efficiency that defines the scintillation yield. These include the donor emission lifetime and donor-acceptor spectral overlap, among others. Another opportunity for future improvements pertains to the efficiency of triplet-triplet exchange interactions via Dexter energy transfer. Currently, the highest-performing PSD-capable plastic scintillators are achieved by loading styrenic polymers with high concentrations of small-molecule fluorophores. The required dopant concentration must exceed the percolation threshold of the matrix, and the bimolecular exchange rate must exceed the rate of triplet trapping due to disorder and defects. Thus, ongoing and future work on improved PSD require increasing the triplet-triplet annihilation efficiency while decreasing the triplet exciton trapping rate. Strategies to this end may involve a combination of compositional purity, monodispersity of the host matrix constituents, and/or higher phase stability of small-molecule fluorophore additives. Other objectives also involve improving the thermomechanical properties and long-term stability of solid-state organic scintillators such as crystals and plastics. Chapter 8 will describe strategies towards improving all of the aforementioned objectives in the context of the first principles discussed here.

Acknowledgments This work was supported by the office of Defense Nuclear Nonproliferation, NA-22, NNSA, U.S. Department of Energy. Sandia National Laboratories is a multimission laboratory managed and operated by National Technology and Engineering Solutions of Sandia, LLC, a wholly owned subsidiary of Honeywell International, Inc., for the U.S. Department of Energy's National Nuclear Security Administration under contract DE-NA0003525

References

1. R.C. Sangster, J.W. Irvine Jr., J. Chem. Phys. **24**(4), 670 (1956)
2. H. Kallmann, Natur and Technik **13**, 15 (1947)
3. I. Broser, H. Kallmann, Ann. Phys. (Berlin, Ger.) **438**(3), 317 (1948)
4. P.R. Bell, Phys. Rev. **73**(11), 1405 (1948)
5. S. Niese, J. Radioanal. Nucl. Chem. **241**(3), 499 (1999)

6. Y. Kaschuck, B. Esposito, Nucl. Instr. Methods A **551**(2-3), 420 (2005)
7. T.A. King, R. Voltz, Proc. R. Soc. London, Ser. A **289**(1418), 424 (1966)
8. G. Laustriat, Mol. Cryst. **4**(1-4), 127 (1968)
9. J.B. Birks, J. Phys. B: At., Mol. Opt. Phys. **1**(5), 946 (1968)
10. N. Zaitseva, L. Carman, A. Glenn, R. Hatarik, S. Hamel, M. Faust, B. Schabes, N. Cherepy, S. Payne, IEEE Trans. Nucl. Sci. **58**(6), 3411 (2011)
11. J.R. Lakowicz, *Principles of Fluorescence Spectroscopy* (Springer, 1999)
12. I.B. Berlman, *Handbook of Fluorescence Spectra of Aromatic Molecules* 2nd edn. (Academic Press, Inc., 1971)
13. I.B. Berlman, *Energy Transfer Parameters of Aromatic Compounds* (Academic Press, Inc., 1973)
14. A.F. Adadurov, P.N. Zhmurin, V.N. Lebedev, V.D. Titskaya, Nucl. Instr. Methods A **599**(2-3), 167 (2009)
15. Eljen Technology website, https://eljentechnology.com/products/plastic-scintillators, last accessed 29.09.2020
16. Saint-Gobain Crystals website, https://www.crystals.saint-gobain.com/products/plastic-scintillators, last accessed 29.09.2020
17. A. Muratsugu, J. Watanabe, S. Kinoshita, J. Chem. Phys. **140**(21), 214508 (2014)
18. A. Arulchakkaravarthi, N. Balamurugan, R. Kumar, P. Santhanaraghavan, S. Muralithar, T. Nagarajan, P. Ramasamy, Mater. Lett. **58**(7-8), 1209 (2004)
19. N. Zaitseva, A. Glenn, L. Carman, H.P. Martinez, R. Hatarik, H. Klapper, S. Payne, Nucl. Instr. Methods A, **789**, 8 (2015)
20. G.W. Robinson, Proc. Natl. Acad. Sci. U. S. A. **49**(4), 521 (1963)
21. N. Karl, in *Organic Electronic Materials*, vol. 41, ed. by R. Farchioni, G. Grosso. Springer Series in Materials Science (Springer-Verlag, Berlin Heidelberg, 2001), pp. 283-326
22. P.L. Feng, M.E. Foster, IEEE Trans. Nucl. Sci. **60**(4), 3142 (2013)
23. T. Vehoff, B. Baumeier, A. Troisi, D. Andrienko, J. Am. Chem. Soc. **132**(33), 11702 (2010)
24. R.A. Weldon Jr., J.M. Mueller, C. Awe, P. Barbeau, S. Hedges, L. Li, M. Mishra, J. Mattingly, Nucl. Instr. Methods A **977**, 164178 (2020)
25. P. Schuster, E. Brubaker, Nucl. Instr. Methods A **859**, 95 (2017)
26. F. Duan, J. Guojun, *Introduction to Condensed Matter Physics*, vol. 1 (World Scientific Publishing, 2005) p. 109
27. B. Ghanbarian, P. Cheng, J. Power Sources **307**, 613 (2016)
28. M.G. Schorr, F.L. Torney, Phys. Rev. **80**(3), 474 (1950)
29. L. Chen, R. Batra, R. Ranganathan, G. Sotzing, Y. Cao, R. Ramprasad, Chem. Mater. **30**(21), 7699 (2018)
30. T. Nishihara, M. Kaneko, Makromol. Chem. **124**(1), 84 (1969)
31. M.S. Healy, J.E. Hanson, J. Appl. Polym. Sci. **104**(1), 360 (2007)
32. P. de Sainte Claire, J. Phys. Chem. B **110**(14), 7334 (2006)
33. J.B. Birks, Nature **214**, 1187 (1967)
34. R. Casillas, M. Adam, P.B. Coto, A.R. Waterloo, J. Zirzlmeier, S. Rajagopala Reddy, F. Hampel, R. McDonald, R.R. Tykwinski, M. Thoss, D.M. Guldi. Adv. Energy Mater. **9**(2), 1802221 (2019)
35. S. Mutsamwira, E.W. Ainscough, A.C. Partridge, P.J. Derrick, V.V. Filichev, Chem. – Eur. J. **22**(30), 10376 (2016)
36. C. Ye, V. Gray, J. Mårtensson, K. Börjesson, J. Am. Chem. Soc. **141**(24), 9578 (2019)
37. F.D. Brooks, R.W. Pringle, B.L. Funt, IRE Trans. Nucl. Sci. **7**(2–3), 35 (1960)
38. N. Zaitseva, B.L. Rupert, I. Pawełczak, A. Glenn, H.P. Martinez, L. Carman, M. Faust, N. Cherepy, S. Payne, Nucl. Instr. Methods A **668**, 88 (2012)
39. N.P. Zaitseva, A.M. Glenn, A.N. Mabe, M.L. Carman, C.R. Hurlbut, J.W. Inman, S.A. Payne, Nucl. Instr. Methods A **889**, 97 (2018)

40. A. Lim, G. Hernandez, J. Latta, H.A. Yemam, W. Senevirathna, U. Greife, A. Sellinger, ACS Appl. Polym. Mater. **1**(6), 1420 (2019)
41. Y. Zhu, Y. Chen, L. Zhang, W. Li, B. Huang, J. Wu, Chem. Eng. Res. Des. **104**, 32 (2015)
42. K. Jin, L. Li, J.M. Torkelson, Polymer **115**, 197 (2017)
43. G.H.V. Bertrand, M. Hamel, F. Sguerra, Chem. – Eur. J. **20**(48), 15660 (2014)
44. H.A. Yemam, A. Mahl, J.S. Tinkham, J.T. Koubek, U. Greife, A. Sellinger, Chem. – Eur. J. **23**(37), 8921 (2017)
45. M. Grodzicka-Kobylka, T. Szczesniak, M. Moszynski, K. Brylew, L. Swiderski, J.J. Valiente-Dobón, P. Schotanus, K. Grodzicki, H. Trzaskowska, J. Instrum. **15**, P03030 (2020)
46. M. Sénoville, F. Delaunay, M. Pârlog, N.L. Achouri, N.A. Orr, Nucl. Instr. Methods A **971**, 164080 (2020)
47. C. Malgrange, C. Ricolleau, M. Schlenker, *Symmetry and Physical Properties of Crystals* (Springer, Dordrecht, 2014)
48. H.-E. Tresca, C.R. Acad. Sci. Paris **59**, 754 (1864)
49. W. Prager, *Introduction to the Mechanics of Continua* (Dover Publications Inc., Mineola, New York, 1961)
50. R. Hill, *The Mathematical Theory of Plasticity* (Clarendon Press, 1950)
51. D.J. Luscher, F.L. Addessio, M.J. Cawkwell, K.J. Ramos, J. Mech. Phys. Solids **98**, 63 (2017)
52. K.M. Davoudi, J.J. Vlassak, J. Appl. Phys. **123**(8), 085302 (2018)
53. M. Li, W. Cui, M.S. Dresselhaus, G. Chen, New J. Phys. **19**, 013033 (2017)
54. Inrad Optics website, https://inradoptics.com/, last accessed 29.09.2020
55. C. Redding, A. Hackett, M. Laubach, R. Feng, P. Feng, C. Hurlbut, P. Liaw, J.P. Hayward, Nucl. Instr. Methods A **954**, 161448 (2020)
56. R.J. Cameron, B.G. Fritz, C. Hurlbut, R.T. Kouzes, A. Ramey, R. Smola, IEEE Trans. Nucl. Sci. **62**(1), 368 (2015)
57. P.B. Rose Jr., A. Okowita, M.J. Lance, E. Sword, IEEE Trans. Nucl. Sci. **67**(7), 1765 (2020)
58. M. Loyd, M. Pianassola, C. Hurlbut, K. Shipp, L. Sideropoulos, K. Weston, M. Koschan, C.L. Melcher, M. Zhuravleva, Nucl. Instr. Methods A **922**, 202 (2019)
59. N.R. Myllenbeck, S. Payne, P.L. Feng, Nucl. Instr. Methods A **954**, 161782 (2020)
60. K. Takasaki, H. Kobayashi, H. Suzuki, S. Ushigome, J. Nucl. Sci. Technol. **47**(3), 255 (2010)
61. L. Bläckberg, A. Fay, I. Jõgi, S. Biegalski, M. Boman, K. Elmgren, T. Fritioff, A. Johansson, L. Mårtensson, F. Nielsen, A. Ringbom, M. Rooth, H. Sjöstrand, M. Klintenberg, Nucl. Instr. Methods A **645**(1), 84 (2011)
62. A. Mahl, A. Lim, J. Latta, H.A. Yemam, U. Greife, A. Sellinger, Nucl. Instr. Methods A **884**, 113 (2018)
63. J.S. Vrentas, C.M. Vrentas, J. Appl. Polym. Sci. **42**, 1931 (1991)
64. T.A. Laplace, B.L. Goldblum, J.E. Bevins, D.L. Bleuel, E. Bourret, J.A. Brown, E.J. Callaghan, J.S. Carlson, P.L. Feng, G. Gabella, K.P. Harrig, J.J. Manfredi, C. Moore, F. Moretti, M. Shinner, A. Sweet, Z.W. Sweger, J. Instrum. **15**, 11020 (2020)

About the Author

Dr. Patrick Feng is a Principal Member of the Technical Staff at Sandia National Laboratories in Livermore, CA. His research is concerned with the development of novel organic-based scintillator materials. Dr. Feng's relevant contributions include the elucidation of fundamental scintillation phenomena in Metal-Organic Frameworks (MOFs), discovery of triplet-harvesting plastic scintillators for spectrally-resolved particle discrimination, development of metal-loaded plastic scintillators for gamma-ray spectroscopy, aging-resistant plastic scintillators, and melt-cast organic glasses for neutron/gamma discrimination. He has nineteen years of synthetic chemistry experience that includes eleven years of organic scintillator development.